frontiers | Frontiers in Earth Science

ORIGINAL RESEARCH
published: 22 July 2022
doi: 10.3389/feart.2022.905852

Isotopic and Hydrogeochemical Characteristics and Genesis of Warm Springs in the Jiangcang Basin, Qinghai, China

Lingxia Liu[1,2,3], *Shihua Qi*[1], *Yongbin Zhang*[4], *Ming Gao*[2], *Jing Hu*[5] *and Wenzhong Wang*[1,2]*

[1]School of Environmental Studies, China University of Geosciences, Wuhan, China, [2]Institute of Hydrogeology and Environmental Geology, Chinese Academy of Geological Sciences, Shijiazhuang, China, [3]Technology Innovation Center for Geothermal & Hot Dry Rock Exploration and Development, Ministry of Natural Resources, Shijiazhuang, China, [4]New Energy Geological Team of Hebei Coalfield Geological Bureau, Xingtai, China, [5]Jiangsu University of Science and Technology, Zhenjiang, China

OPEN ACCESS

Edited by:
Wenjing Lin,
Chinese Academy of Geological Sciences, China

Reviewed by:
Kunal Singh,
Geological Survey of India, India
Jianfei Yuan,
Chengdu Geological Survey Center, China

***Correspondence:**
Wenzhong Wang
308200378@qq.com

Specialty section:
This article was submitted to Geochemistry, a section of the journal Frontiers in Earth Science

Received: *28 March 2022*
Accepted: *03 June 2022*
Published: *22 July 2022*

Citation:
Liu L, Qi S, Zhang Y, Gao M, Hu J and Wang W (2022) Isotopic and Hydrogeochemical Characteristics and Genesis of Warm Springs in the Jiangcang Basin, Qinghai, China. Front. Earth Sci. 10:905852. doi: 10.3389/feart.2022.905852

The Jiangcang Basin is a Cenozoic faulted basin, where many low-temperature warm springs are exposed, with the highest temperature being 36.6°C. The study of the hydrogeochemical characteristics of the geothermal fluids of these warm springs can effectively clarify the genetic mechanisms of the geothermal resources in the Jiangcang Basin and thus is of great significance for the development and utilization of geothermal resources in the Qinghai Province. Using the geothermal and geological conditions of the Jiangcang Basin, this study analyzed the hydrochemical and isotopic characteristics of water samples collected from cold water and from four warm springs in the Jiangcang Basin, obtaining the following results. The four warm springs have the hydrochemical types of HCO_3-Ca·Mg, HCO_3-Ca·Na·Mg, and HCO_3·SO_4-Na·Ca and total dissolved solids (TDSs) of 720.4–1,663 mg/L. Moreover, no significant positive correlation is found between Cl^- and other ions in the warm springs. The results of isotopic analysis show that the warm springs are mainly recharged by atmospheric precipitation and meltwater from ice and snow, with a recharge elevation of 4,401–4,501 m. Furthermore, the geothermal reservoirs in the Jiangcang Basin have temperatures of 51–83°C and circulation depths of 1,848–2,610 m. Atmospheric precipitation and the meltwater from ice and snow infiltrate downward in high mountain areas and form runoffs along the tectonic channels in the basin. After being heated through deep circulation, they migrate upward along fault fracture zones under the influence of faults and the water blocking of mudstones, during which they cool by thermal conduction and mixing with shallow cold groundwater. Finally, the mixed water is exposed in the form of low-temperature tectonic warm springs. The results of this study can provide data for the exploitation and utilization of geothermal resources in the Qinghai Province.

Keywords: Jiangcang Basin, hydrogeochemistry, Silica geothermometers, geothermal reservoir temperature, geothermometer, isotope

1 INTRODUCTION

Eco-friendly and sustainable development is the common pursuit of all human beings. Geothermal resources, a source of renewable new clean energy that can be directly utilized, have great potential for development. China is rich in geothermal resources, with 2,334 discovered warm spring outcrops and 5,818 existing geothermal exploitation wells (Wang G. L. et al., 2017). In recent years, many researchers have investigated geothermal resources in China, especially with reference to their occurrence regularity, hydrogeochemical characteristics, and genetic modes (Guo et al., 2015; Du et al., 2012; Wang G.L. et al., 2017; Yuan et al., 2020).

The Qinghai Province, located in the northeast of the Qinghai-Tibet Plateau, features complex geological structures and strong neotectonic movements. It is rich in geothermal resources due to its numerous geothermal anomalous areas, including more than 200 geothermal sites (Zhang, 1999). Much work has been conducted on the geothermal resources in Qinghai. For example, Zhang et al. (2007) analyzed the genetic mechanisms of the geothermal water in the Dujiazhuang geothermal field in Xining, Qinghaim using the Langelier-Ludwig diagram combined with isotopic and hydrological analyses. The results show that geothermal water from the Dujiazhuang geothermal field is of meteoric origin and is recharged by modern water. Moreover, the geothermometers indicate that there are geothermal reservoirs in the Dujiazhuang geothermal field whose temperature is far higher than that of geothermal well DR 2005 (i.e., 62.5°C). Li et al. (2007) analyzed the recharge sources and genesis of Yaoshuitan warm spring based on hydrochemical characteristics and stable isotopes. Sun et al. (2019) obtained the circulation mechanisms of the geothermal water in the Xining Basin based on the study of the dynamic, chemical, and geothermal fields of groundwater, as well as the isotopic characteristics. Sun et al. (2022) determined the genetic mechanisms for the high TDS of different geothermal water bodies in the Xining Basin through the TDS and hydrochemical analyses. Wang (2009) systematically studied the hydrochemical characteristics of geothermal water in the Qiabuqia area and their regional distribution. They also estimated the geothermal reservoir temperature in this area using geochemical geothermometry, thus providing basic data and a scientific basis for the exploitation of geothermal resources in this area. Li (2016) analyzed the hydrogeochemical and isotopic characteristics and the genesis of the geothermal water in the Qiabuqia area. They inferred that the geothermal water in the Qiabuqia area originates from the confined water in the west and the meltwater from ice in the high mountains in the north, and the heat is mainly derived from the mantle through thermal conduction. Tang et al. (2020) analyzed the tectonic background and heat source mechanisms of the Gonghe Basin in Qinghai using isotope chronology and hydrogeochemistry. Consequently, they proposed a ternary heat accumulation model of hot dry rocks in the Gonghe Basin. Ma et al. (2020) analyzed the migration pattern and genetic mechanisms of geothermal fluids in the Gonghe Basin through hydrogeochemical analysis. Lang et al. (2016) analyzed the hydrochemical and stable isotopic characteristics of the geothermal fluids in the Guide Basin. They also estimated the temperature and circulation depth of the geothermal reservoirs in the geothermal fields in the Guide Basin and identified the genetic mechanisms of the geothermal fields. Li et al. (2016a) investigated the characteristics of the geothermal reservoirs and the geothermal field, as well as the hydrogeochemical characteristics of geothermal water in the Guide Basin. Based on these characteristics, they summarized the occurrence regularity and the geological genetic modes of the geothermal resources in the Guide Basin. Jiang et al. (2019) developed an isotopic migration module based on the water-heat-rock coupling model. Using this module, they simulated the isotopic fractionation of δ^2H and $\delta^{18}O$ induced by advection, diffusion, and water-rock interaction and analyzed the recharge sources and rates and the temperature of geothermal water in the basin. Dai (2020) investigated convective geothermal water along five faults in the Guide Basin. Then, they analyzed the genetic mechanisms of the geothermal resources in the basin, based on the hydrochemical and stable isotopic characteristics to deepen the understanding of the circulation process of the geothermal water in the basin.

Studies of the geothermal resources in the Qinghai Province focus on basins with a low elevation (<3,000 m), such as the Gonghe, Xining, and Guide basins, while the geothermal resources in the basins with a high elevation (>3,800 m), such as the Jiangcang and Reshui basins, lying in the upper reach of the Datong River, have been scarcely concerned. Previous surveys reveal that four warm springs are exposed in the Jiangcang Basin. Among them, the Muliqugu warm spring located on the south slope of the Tuolai Nanshan Mountain on the north bank of the Datong River has the highest temperature of 36.6°C (Li et al., 2016b). According to the report entitled Current Status Assessment and Zoning of Geothermal Resources in Qinghai Province (2015), the Jiangcang Basin has considerable potential for exploration and has been explored recently (Yang et al., 2015). Given this, this study analyzed the chemical composition and recharge sources and revealed the genetic mechanisms of the geothermal water in the Jiangcang Basin based on the hydrogeochemical characteristics of the geothermal water. The purpose is to provide a scientific basis for the future exploitation and utilization of the geothermal resources in Qinghai.

2 OVERVIEW OF THE STUDY AREA

The Jiangcang Basin is located in the northeast of the Qinghai Province and lies at the junction of Gangcha County, Qilian County, and Tianjun County, Haixi. This basin features abundant resources, large grasslands, a sparse population, and an underdeveloped economy and non-mainstream culture. The Tibetans living have a nomadic economy. The study area has a typical plateau continental climate, which is characterized by indistinct seasons, cold climate, and large temperature variations. This basin has an average annual temperature of −1.93–0.5°C, average annual precipitation of 463 mm, and average annual evaporation of 1,261 mm. Moreover, the period from June to August is the rainy season and the period from January to May is

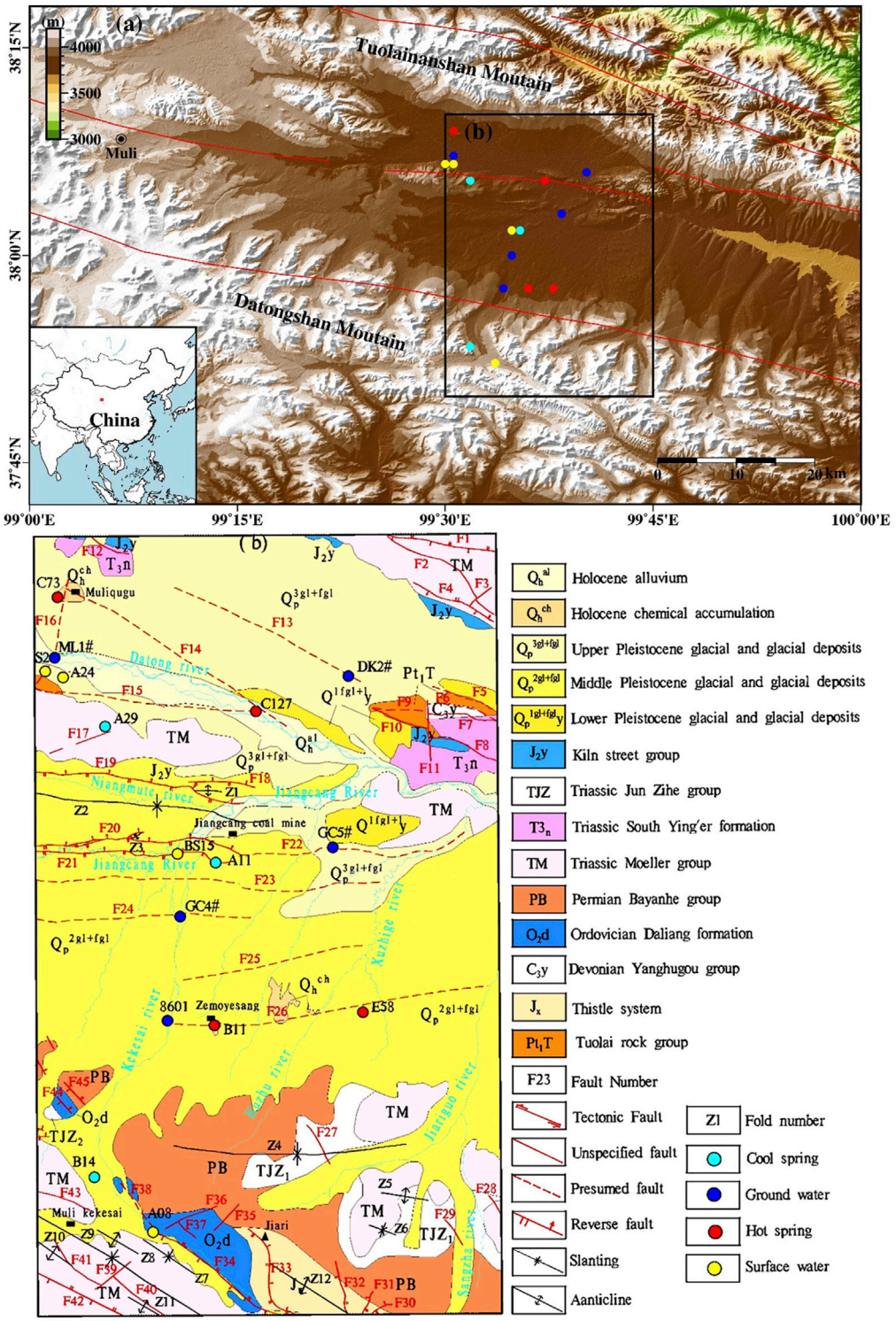

FIGURE 1 | (A) Geological sketch and sampling point location map of the study area. **(B)** After hydrogeological and environmental geological survey of Qinghai energy.

dominated by snow. This basin suffers from inconvenient transportation, with only the west-east Reshui Industrial Park—Jiangcang and the north-south Gangca-Jiangcang highways passing through it.

The study area is a part of the middle part of the Proterozoic Qilian paleocontinental block in the western craton. It is sandwiched between large fault zones, with one extending from the south slope of the Tuolai Mountain to Lenglongling and the other from the Shule Nanshan Mountain to Datong Mountain (**Figure 1A**), and it lies in the Muli-Jiangcang-Reshui basin (also referred to as the MJR Basin). The crystalline basement of the study area consists of Paleozoic mesometamorphic rocks, and the cap rock is a set of Carboniferous-Jurassic clastic sedimentary suites. The folds of the MJR Basin are a synclinorium with an axial direction of NW-SE, approximately the same as the strike of the Qilian Mountains overall.

Under the influence of regional tectonism, the structures in the major areas of the Jiangcang Basin are dominated by faults, followed by folds. Specifically, there are 45 faults and 12 folds in the study area (**Figure 1B**). Among these, faults F13, F14, and F15, on both banks of the Datong River, and faults F34, F40, and F42, on the southwest side of the study area, extend NW-SE strike, which is the same as the direction of the regional tectonic line. The faults from the south of the Datong River to the north of the Zemoyesang Spring show a west-east strike. The major faults between the Datong Rive and the Jiangcang mining area are dominated by reverse faults, including F18, F19, F20, and F21. Moreover, several inferred deep faults, namely F22, F23, F24, F25, and F26, exist between the Jiangcang mining area and the Zemoyesang Spring. Faults F34 and F42, lying in the southwest, serve as the boundary faults of the central Qilian uplift zone and the southern Qilian geosyncline zone. These two faults have a large scale and show long-term activity. Each of them has a total regional length of hundreds of km and extends eastward. They are intruded by Caledonian mafic rocks and thus cut deeply (Li, 1952).

Muliqugu warm spring C73 and the C127 warm spring in a floodplain of the Datong River extend in the NWW direction along fault F14. Among them, C73 is exposed at the junction of F14—a major compressive deep fault with a NWW strike—and F16—a NNE-strike compressive fault; C127 is exposed in the superimposition part of two NWW-strike major compressive fractures F14 and F15. Warm springs B11 and E58, which have a NEE-SWW strike, are exposed in F26, a concealed regional fault with a strike of approximately 5° at the junction of the Jiangcang Basin and the Datong Mountains. There are six spring vents along this fault at the early stage (Xie et al., 1987), with a large amount of sinter exposed on the surface. Cold springs A11 and A29 are exposed in fault zones F21 and F17, respectively.

The outcrops in the study area include Proterozoic, Sinian, Ordovician, Carboniferous, Permian, Triassic, Jurassic, Paleogene, Neogene, and Quaternary strata, among which the Triassic and Jurassic strata are well preserved and widely distributed.

3 SAMPLES AND EXPERIMENTAL METHODS

A total of 21 sets of water samples were collected in this study, including four sets from warm springs, three sets from cold spring waters, six sets from surface water, four sets from groundwater, and three sets of snow samples (**Figure 1A**). Before the sampling, field physical and chemical parameters, such as pH, water temperature (T), and electrical conductivity (EC), were measured *in situ*. Samples were collected after these parameters became stable. All of the samples were stored in polyethylene bottles, kept refrigerated, and sent to labs for analyses in time.

The total analysis, trace element analyses, and δ^2H and $\delta^{18}O$ measurements of the water samples were carried out at the Key Laboratory of Groundwater Science and Engineering, Ministry of Land and Resources, Institute of Hydrogeology and Environmental Geology, Chinese Academy of Geological Sciences. Major anions (K^+, Na^+, Ca^{2+}, and Mg^{2+}) and trace components were determined using a Perkin Elmer Optima 8000 inductively coupled plasma optical emission spectrometer (ICP-OES; ± 1%). Cl^-, SO_4^{2-}, and F^- were measured using a Dionex ICS-1100 ion chromatography system, with a testing error of ±1%. The HCO_3^- concentration was analyzed using the reagent titration method, with an analytical precision of ±2%. Moreover, silicates were determined using a SHIMADZU UV-2550 spectrophotometer, with testing errors of less than 0.0003%. All the water samples were tested for cation-anion balance. As a result, all the samples yielded charge-balance errors of within ±5%, except for B14, which had a charge-balance error of 5.61%, thus meeting the demands for testing precision. δ^2H and $\delta^{18}O$ measurements were conducted using a high-precision Picarro L2130-I isotope analyzer, with a measurement precision of 0.025% (**Table 1**).

4 RESULTS AND DISCUSSION

4.1 Hydrochemical Characteristic

4.1.1 TDS

TDS intensively reflects the major ions in groundwater and is an important indicator of the chemical characteristics of groundwater. The TDS of water samples from the surface water was 227.1–388.5 mg/L (average: 262.1 mg/L), and that of water samples from the groundwater was 178.1–354.6 mg/L (average: 258.3 mg/L). As for the cold springs in the study area, water samples from B14 had high TDS, while those from the A11 and A29 had TDS of 270.4 mg/L and 356.8 mg/L, with an average of 313.6 mg/L. Water samples from warm springs C73, C127, E58, and B11 in the study area had a TDS range of 720.4–1,663 mg/L, with an average of 1,234.6 mg/L. Therefore, the warm springs have the highest TDS, followed by the cold springs and surface water, while the surface water have the lowest TDS in the study area (**Table 1**).

TABLE 1 | Chemical composition and hydrogen and oxygen isotope composition of water samples.

Type	Sample ID	pH	Temperature(°C)	Hydrochemical composition/(mg/L)											Hydrochemical type	Isotope/‰		Charge balance (%)
				Ca^{2+}	Mg^{2+}	Na^{+}	K^{+}	HCO_3–	SO_4^{2}–	Cl^{-}	F^{-}	TDS	H_2SiO_3	Li	Sr		δD	$\delta^{18}O$	
Hot spring	C73	5.93	36.6	105.10	38.87	91.08	12.78	612.90	29.70	71.78	2.00	720.4	51.61	0.146	0.692	HCO_3-Ca·Na·Mg	–60	–8.9	–0.12
	C127	6.46	6.9	267.60	92.50	172.50	74.55	1,474.00	56.74	165.30	1.10	1,663.0	52.13	0.975	2.854	HCO_3-Ca·Mg	–60	–8.3	1.45
	E58	6.66	19.5	166.80	68.40	202.10	33.41	836.50	320.30	79.48	2.40	1,322.0	26.88	0.708	2.196	HCO_3·SO_4-Na·Ca	–59	–9.1	3.98
	B11	5.94	24.0	141.30	73.89	163.20	18.79	770.10	321.10	59.8	1.40	1,233.0	32.81	0.466	1.143	HCO_3-Ca·Mg	–63	–10.0	–1.30
Cold spring	A11	6.80	1.8	40.68	9.00	41.94	1.11	147.80	90.05	3.27	0.20	270.4	7.96	0.014	0.231	HCO_3·SO_4-Ca·Na	–42	–7.1	3.75
	A29	6.40	2.4	61.53	15.14	45.23	1.52	239.30	97.67	5.55	—	356.8	9.67	0.008	0.466	HCO_3·SO_4-Ca·Na	–42	–6.3	2.87
	B14	6.97	1.4	3.48	0.96	867.40	0.89	29.85	1,680.00	15.03	—	2,583.0	—	—	—	SO_4-Na	–51	–8.7	5.61
Surface water	A24	7.62	—	26.85	8.66	39.30	1.02	104.70	87.19	2.29	—	227.1	9.78	0.007	0.470	SO_4·HCO_3-Na·Ca	—	—	–2.24
	A08	7.34	—	34.02	8.14	34.25	0.82	104.70	85.29	4.63	—	228.0	5.51	—	0.167	SO_4·HCO_3-Ca·Na	—	—	1.36
	S2	7.90	—	68.39	16.56	26.53	1.83	233.70	83.75	8.75	0.16	345.9	4.54	0.021	0.461	HCO_3·SO_4-Ca	–48	–7.6	–2.14
	BS15	7.61		63.07	10.37	64.38	0.85	232.80	115.80	7.52	0.12	388.5	9.15	—	0.233	HCO_3·SO_4-Ca·Na	–27	–4.6	1.55
	BS19	7.50		39.04	5.44	49.91	0.82	131.30	101.00	4.10	0.12	238.7	5.41	—	0.207	HCO_3·SO_4-Na·Ca	–43	–7.1	0.92
	AS03	7.34		34.02	8.14	34.25	0.82	104.70	85.29	4.63	<0.1	228.0	5.51	—	0.167	SO_4·HCO_3-Ca·Na	–50	–8.4	1.36
Groundwater	DK2#	7.27	—	63.73	13.54	5.32	1.42	233.7	13.99	9.10	0.18	240.3	12.21	0.011	0.303	HCO_3-Ca·Mg	–46	–6.8	1.87
	GC4#	7.65	—	41.62	14.57	21.17	4.07	150.80	30.36	23.10	0.22	260.1	27.14	0.011	0.348	HCO_3-Ca·Mg	–32	–4.9	2.32
	GC5#	7.76	—	56.53	17.18	45.22	2.88	199.4	88.45	35.36	0.12	354.6	8.06	0.360	56.53	HCO_3·SO_4-Ca·Na	–58	–9.0	2.62
	ML1#	7.61	—	47.19	14.63	5.13	1.76	214.0	6.92	4.90	0.38	178.1	8.38	0.030	0.197	HCO_3-Ca·Mg	–49	–8.0	–0.31
Snow	A-19	7.17	—	10.46	0.60	302.00	0.34	47.76	599.40	5.13	—	942.3	—	—	—	SO_4-Na	–38	–6.4	2.14
	ADX-02	6.45	—	1.57	0.17	86.83	0.06	8.63	167.10	1.78	0.10	266.0	5.41	—	—	SO_4-Na	–32	–7.2	1.27
	ADX-03	6.57	—	1.99	0.21	101.30	0.08	11.51	214.40	1.78	—	325.9	—	—	—	SO_4-Na	–42	–7.2	–4.06

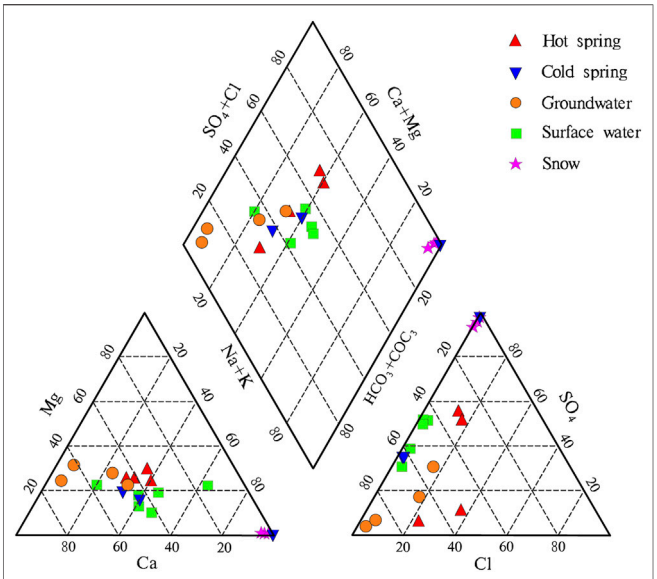

FIGURE 2 | Piper trilinear diagram of the water samples from the Jiangcang Basin.

4.1.2 Hydrochemical Types

The hydrochemical types of groundwater can comprehensively reflect the primary hydrogeochemical environment of groundwater, including occurrence conditions of groundwater, water-rock interaction, and recharge-drainage circulation. To understand the hydrochemical characteristics of warm springs and their genetic mechanisms, the authors determined the hydrochemical types of different types of water bodies using the Shukalev classification method. The Piper trilinear diagram was plotted according to hydrochemical data (**Figure 2**). This plot can effectively reflect the differences in the hydrochemical types of warm spring water, cold water, and meltwater from snow.

Water samples from the four warm springs had pH of 5.94–6.66, with an average of 6.20, indicating that they were weakly acidic. As for the warm springs from the study area, the water samples from C127 and B11 yielded hydrochemical types of HCO_3-Ca·Mg, and those from C73 and E58 yielded hydrochemical types of HCO_3-Ca·Na·Mg and HCO_3·SO_4-Na·Ca, respectively. The water samples from cold springs A11, A29, and B11 had pH values of 6.408.05, with an average of 7.08. The water samples from A11 and A29 showed a hydrochemical type of HCO_3·SO_4-Ca·Na, and those from B14 located in the front of the Datong Mountains had a hydrochemical type of SO_4-Na. The surface water samples had pH of 7.34–7.90, with an average of 7.48. The surface water samples close to the piedmont had hydrochemical types of SO_4·HCO_3-Na·Ca and SO_4·HCO_3-Ca·Na, while those close to the center of the Jiangcang Basin had hydrochemical types of HCO_3·SO_4-Ca·Na, HCO_3·SO_4-Na·Ca, and HCO_3·SO_4-Ca. The groundwater samples had pH of 7.61–7.76, with an average of 7.69. Water samples from wells DK2#, GC4#, and ML1#, all of which had depths greater than 100 m showed a hydrochemical type of HCO_3-Ca·Mg, while those from well GC5# with a small depth of 13.5 m had a hydrochemical type of HCO_3·SO_4-Na·Ca. The three meltwater samples from snow had a hydrochemical type of SO_4-Na. Because these samples were collected around the Jiangcang mining area, it is inferred that they were affected by coal dust.

The analysis indicated that most of the surface water, shallow groundwater, and cold spring water in the study area had similar hydrochemical types, and they are mainly recharged by atmospheric precipitation and meltwater from ice and snow. Moreover, due to the short circulation pathway, they are renewed at a high rate. Cold spring B14, which is close to the piedmont, have the same hydrochemical type as the meltwater from snow, indicating that B14 is mainly recharged by the meltwater from snow. Warm springs C127 and B11 have the same hydrochemical type as the deep groundwater—HCO_3-Ca·Mg, indicating that C127, B11, and the deep groundwater are deeply circulating confined water. Warm spring E58 has similar hydrochemical type to the cold springs. However, the warm springs have significantly higher Cl^- concentration than cold springs and generally higher TDS than cold water (i.e., water other than warm spring water).

The differences in the hydrochemical types and TDS of the geothermal water indicate differences in the degree of water-rock interaction. Specifically, the water-rock interaction in the geothermal water is greater than that the cold water.

4.1.3 Characteristics of the Trace Elements

The trace elements in the water samples from the warm springs mainly included fluorine (F), metasilicic acid, lithium (Li), and strontium (Sr). As shown in **Table 1**, water samples from the cold and warm springs showed F^- concentrations of 0–0.38 mg/L (average: 0.18 mg/L) and 1.10–2.40 mg/L (average: 1.73 mg/L), respectively, with the latter 9.6 times the former. They had metasilicic acid concentrations of 4.54–27.14 mg/L (average: 9.89 mg/L) and 26.88–52.13 mg/L (average: 40.86 mg/L), with the latter 4.1 times the former. Moreover, they had Li concentrations of 0.007–0.030 mg/L (average: 0.015 mg/L) and 0.146–0.975 mg/L (average: 0.574 mg/L), with the latter 38.3 times the former. Therefore, the warm springs have higher trace element concentrations than the shallow cold springs overall, reflecting that they feature deep circulation. Moreover, the metasilicic acid and Li with high concentrations are the indicators of warm spring water. As for the warm springs in the study area, their Sr concentrations meet the criterion for natural mineral water, the F^- concentrations of C73 and E58 meet the criteria for natural mineral water, and the Li concentrations of them except for C73 meet the criterion for natural mineral water. Overall, C127 has the highest water quality among the warm springs. However, all the warm springs are not suitable to use as natural mineral water.

4.1.4 Correlation Between Icons and TDS

As indicated by the analyses of the correlation between the major ions and TDS of the warm springs in the Jiangcang Basin (**Figure 3**), there was a high correlation between icons Mg^{2+}, Ca^{2+}, HCO_3^-, and K^+ and TDS, with a correlation coefficient (R^2) of greater than 0.75. Moreover, Mg^{2+} showed a high R^2 of up to 0.96, while Na^{2+} showed a low R^2 of 0.65. These results reflect the ion composition of medium- and low-temperature thermal

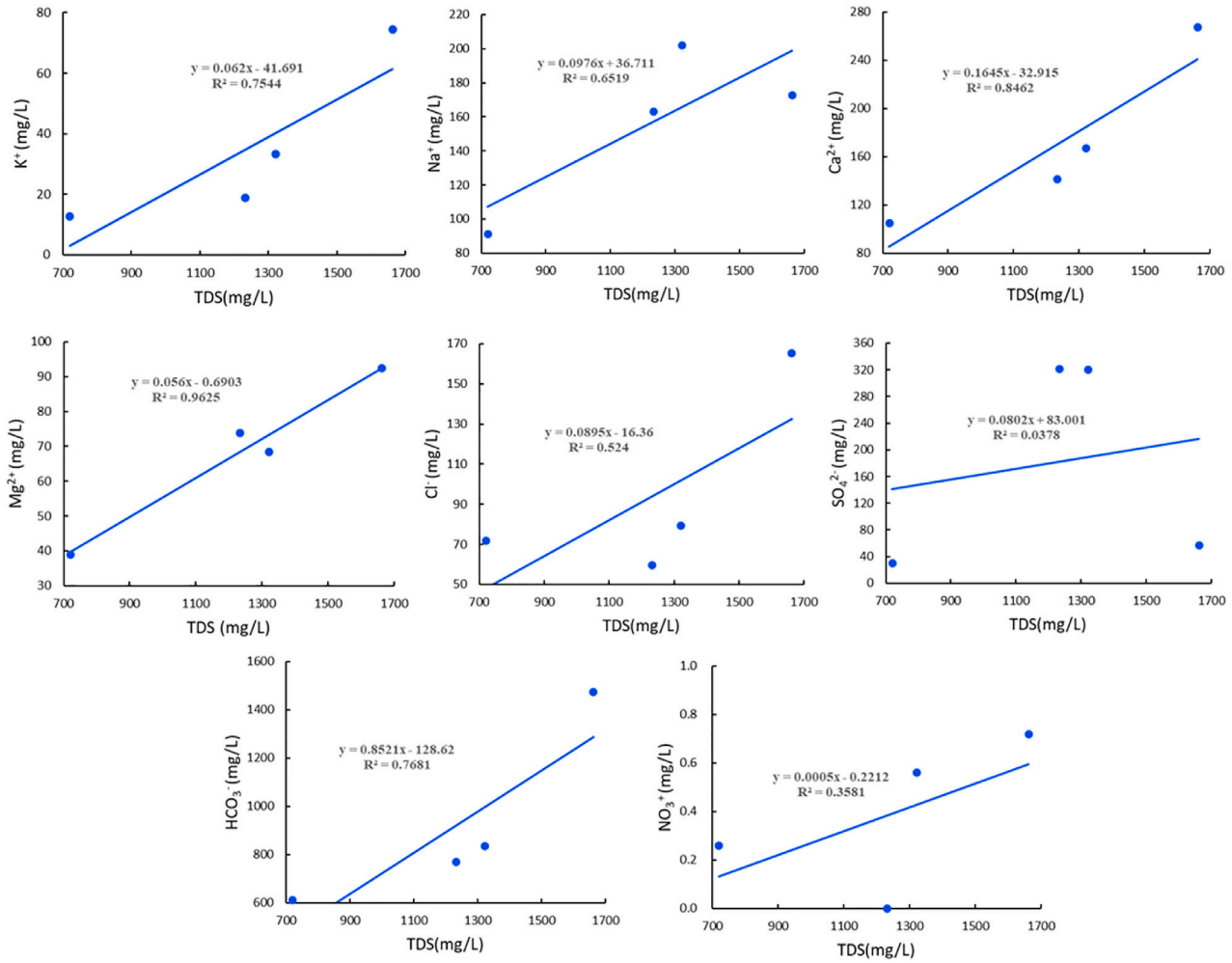

FIGURE 3 | Curves showing the correlation between ions and TDS of water samples from warm springs in the Jiangcang Basin.

springs. Correlation analyses suggested a low correlation between anions and TDS, except for HCO_3^-, which showed an R^2 of 0.77. Moreover, SO_4^{2-} showed the lowest R^2 of 0.04. These results indicate significantly reduced direct recharge by the surface water and the shallow groundwater containing high SO_4^{2-} concentrations, and this significantly enhanced the effects of deep water-rock interaction on the salinity.

Cl^- in groundwater mainly originates from the dissolution of salt or other chlorides in sedimentary rocks, the weathering and dissolution of chlorides in magmas, seawater, the leaching of materials erupting from volcanoes, and man-made pollution. Cl^- is stable since it is not liable to be absorbed or react with other minerals. Therefore, Cl^- can be used to trace other ions to which it is closely related in order to analyze groundwater runoff.

As shown by the analyses of the correlation between Cl^- and other ions (**Figure 4**), there was no significant positive correlation between Cl^- and other ions. This result indicates that the trace elements in the warm springs in the Jiangcang Basin mainly originate from the dissolution of relevant minerals. Moreover, there was a positive correlation between the Na^+ concentration and the length of the runoff pathways of groundwater. Specifically, a higher Na^+ concentration corresponds to longer runoff pathways in the warm springs (e.g., E58). Metaboric acid (HBO_2) widely exists in the formation and migration of groundwater, and the precipitation and dissolution of boron-bearing minerals in water-rock interaction are closely related to groundwater runoff. In detail, the boron content decreases with increased runoff intensity of geothermal fluids (Yuan. 2010). The water samples from the warm springs in the Jiangcang Basin had a high HBO_2 content, 60 times that of the water samples from the cold springs. This finding indicates that the geothermal water in the basin features small and low-rate runoff. Moreover, the high TDS also indicates strong water-rock interaction.

4.2 Characteristics of Stable Hydrogen and Oxygen Isotope

4.2.1 Recharge Sources of Warm Springs

Stable hydrogen and oxygen isotopes (δ^2H, $\delta^{18}O$) help distinguish groundwater origin, identify the hydraulic

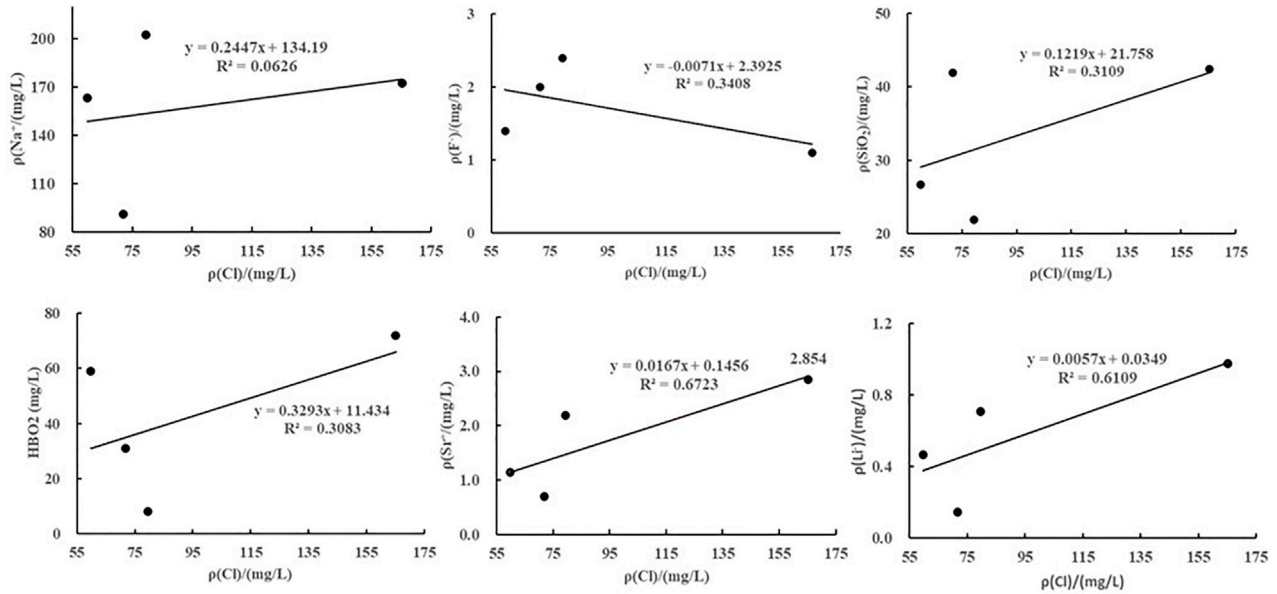

FIGURE 4 | Curves showing the relationships between the ions and Cl^- in the warm springs in the Jiangcang Basin.

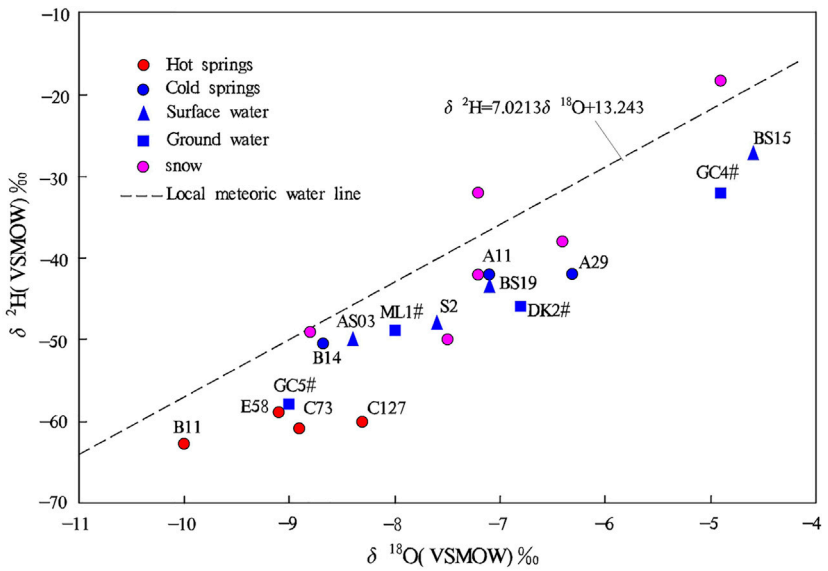

FIGURE 5 | δ^2H vs. $\delta^{18}O$ relationship of water samples from the Jiangcang Basin.

connections among atmospheric precipitation, surface water, and groundwater, trace groundwater recharge conditions, and explore groundwater circulation pathways. ^2H and ^{18}O are rich in liquid but depleted in gas due to their low vapor tension. As a result, the composition of hydrogen and oxygen isotopes are different in different groundwater circulations (Zhang, 1988). Besides being slightly affected by mixing, the δ^2H value of groundwater is mainly determined by recharge temperature and elevation, while the $\delta^{18}O$ value of groundwater mainly depends on the degree of water-rock interaction and the water-rock ratio (Ni et al., 2016).

Through the 1-D linear regression analyses of δ^2H and $\delta^{18}O$ values of the atmospheric precipitation in the study area, the local meteoric water line (LMWL) equation of the Jiangcang Basin was fitted as follows: $\delta^2H = 7.0213\delta^{18}O + 13.243$ (R2=0.8935, n=7), which approximates the LMWL equation for the Qilian Mountain (Sun et al., 2019) $\delta^2H = 7.77\delta^{18}O + 13.03$ (R2=0.99, n=127). This similarity indicates

that the fitted MWL equation of the Jiangcang Basin is reasonable.

The δ^2H vs. $\delta^{18}O$ curve was plotted based on the data on water samples from the warm springs, cold springs, surface water, groundwater, and precipitation, as shown in **Figure 5**. According to this figure, water samples from the thermal water had δ^2H values of −63‰–−59‰ (average: −60.8‰) and $\delta^{18}O$ values of −10‰–−8.3‰ (average: −9.1‰), and those from the cold springs had δ^2H values of −51‰–−42‰ (average: −45‰) and $\delta^{18}O$ values of −8.7‰–−6.3‰ (average: −7.4‰). Moreover, water samples from the surface water had δ^2H values of −50‰–−27‰ (average: −39.2‰) and −8.4‰–−2.8‰ (average: −6.1‰), and those from the groundwater had δ^2H values of −53‰–−32‰ (average: −45‰) and $\delta^{18}O$ values of −8.3‰–−4.9‰ (average: −7.0‰). As shown in **Figure 5**, all the samples were distributed along the LMWL, indicating that they were mainly recharged by atmospheric precipitation and the meltwater from snow. However, the points of the δ^2H and $\delta^{18}O$ values of all the water samples were located to the right of the LMWL, indicating that $\delta^{18}O$-shift occurred. The surface water samples were close to the LMWL, suggesting that they were mainly recharged by modern atmospheric precipitation across short circulation pathways and with a high rate of renewal. Most groundwater samples were plotted close to the LMWL, and their average δ^2H and $\delta^{18}O$ values were close to those of the surface water samples, suggesting that the groundwater was of meteoric and surface water origin. For example, well GC4# lies in the floodplain of the Kekesaiqu area, and surface river water BS15 is also in this area. **Figure 5** shows that GC4# was recharged by BS15. In addition, water samples from ML1# and DK2# were distributed close to those from cold springs A11 and A29 and surface water S2 and BS19, indicating that the groundwater has similar circulation pathways to cold springs and a higher renewal rate. The groundwater at ML1# and DK2# is mainly recharged by atmospheric precipitation, and it is mixed with large amounts of surface water. Compared with other water samples, samples from the warm springs showed more significant $\delta^{18}O$-shift. In general, the δ^2H value cannot be significantly affected by the hydrogen isotope exchange between water and surrounding rocks. However, the $\delta^{18}O$ value can be increased by the oxygen isotope exchange between water and surrounding rocks, and the rate of the oxygen isotope exchange increases rapidly with increased temperature. Therefore, the degree of $\delta^{18}O$-shift depends on and reflects not only the degree of the oxygen isotope exchange between water and surrounding rocks but also the temperature during the water-rock interaction (Zhang et al., 2021). The average annual $\delta^{18}O$ value of the local atmospheric precipitation is −9.2‰ (Yang, 2019), which is lower than the average $\delta^{18}O$ values of water samples from the cold springs, surface water, and groundwater. This result indicates that cold springs, surface water, and groundwater experienced evaporation. The $\delta^{18}O$ value of the water samples from the warm springs was roughly the same as the average annual $\delta^{18}O$ value of the local atmospheric precipitation, suggesting that the $\delta^{18}O$-shift of the warm springs is caused by water-rock interaction.

TABLE 2 | Calculated elevation of the recharge areas of warm springs.

Warm spring	Sample elevation (m)	δ^2H (‰)	Recharge elevation (m)
C73	3,831	−61	4,451
C127	3,771	−60	4,426
E58	3,851	−59	4,401
B11	3,891	−63	4,501

4.2.2 Recharge Elevation of Warm Springs

In general, the δ^2H and $\delta^{18}O$ values for atmospheric precipitation are linearly related to the temperature. The elevation effect refers to the phenomenon that, with increased elevation, the temperature of air decreases and, accordingly, the δ^2H and $\delta^{18}O$ values of water also decrease (Sun et al., 1992). The reasons are as follows. The air temperature decreases, and the water vapor in air condenses as the elevation increases. Moreover, the increased elevation corresponds to the decreased pressure and volume expansion of air, which also lead to the decreased temperature and the condensation of water vapor in air. The water vapor condensation will cause isotopic fractionation and decreased raindrop evaporation. As a result, precipitation increases on the windward side of a mountain, resulting in the formation of an overtopping precipitation area. Accordingly, the isotope content of clouds decreases with increased elevation, and thus the elevation effect is formed (Chen et al., 2019). The elevation effect of isotopes in the atmospheric precipitation can be used to determine the recharge sources for groundwater and their elevation. However, a $\delta^{18}O$ shift tends to occur in geothermal water due to the water-rock interaction during the deep circulation of geothermal water. As a result, the recharge elevation calculated using $\delta^{18}O$ values will deviate from its actual value. Therefore, in this study, the recharge elevation of the warm springs was determined based on δ^2H values in this study.

The relationship between the δ^2H value and recharge elevation was fitted using the δ^2H and $\delta^{18}O$ values of atmospheric precipitation at different elevation values. The fitted equation is:

$$H = -24.995\,\delta^2H + 2926 \quad (1)$$

where H is recharge elevation.

The fitted equation approximates the elevation effect equation proposed by (Li et al., 2016a), that is, $H=-25.47\,\delta^2H + 2{,}827.68$.

As shown in **Table 2**, the recharge elevation of the four warm springs in the study area was calculated as 4,401–4,501 m, which is approximately 600 m greater than the elevation of the sampling sites. As shown by comparison and analysis based on the terrain and fault distribution in the study area, the recharge areas of the four warm springs are mainly located in the Tuolai Nanshan Mountain and the Datong Mountain, which lie on the north and south sides of the Jiangcang Basin, respectively. In these recharge areas, precipitation and meltwater from snow infiltrate and then are exposed along faults after deep circulation.

4.3 Estimation of Geothermal Reservoir Temperature

The geothermal reservoir temperature is a critical parameter in assessing the formation mechanism of geothermal resources and

TABLE 3 | Formulas for calculation of cationic geothermometers.

Geothermometer	Calculation formula
Na/K	T=1,217/(log(Na/K)+1.483)–273.15
K/Mg	T=4,410/(13.95–log(K^2/Mg))–273.15
Na-K-Ca	$T = \frac{1647}{\log(\frac{Na}{K})+\beta(\log(\frac{\sqrt{Ca}}{Na})+2.06)+2.47} - 273.15$ β=4/3(when t<100°C)or β=1/3(when t>100°C)

TABLE 4 | Temperature of warm springs in the Jiangcang Basin calculated using geothermometers.

Warm spring	Temperature (°C)	$T_{Na/K}$ (°C)	$T_{K/Mg}$ (°C)	$T_{Na-K-Ca}$ (°C)	No-steam loss quartz thermometer (°C)	Chalcedony geothermometer (°C)	Multi-mineral equilibrium (°C)	Temperature (°C)
C73	36.6	247.9	57.8	163.5	91.4	60.7	96	83
C127	6.9	385.6	89.2	229.2	91.8	61.2	53	69
E58	19.5	264.2	73.1	173.5	64.7	32.7	55	51
B11	24	229.4	59.2	154.9	72.4	40.7	85	66

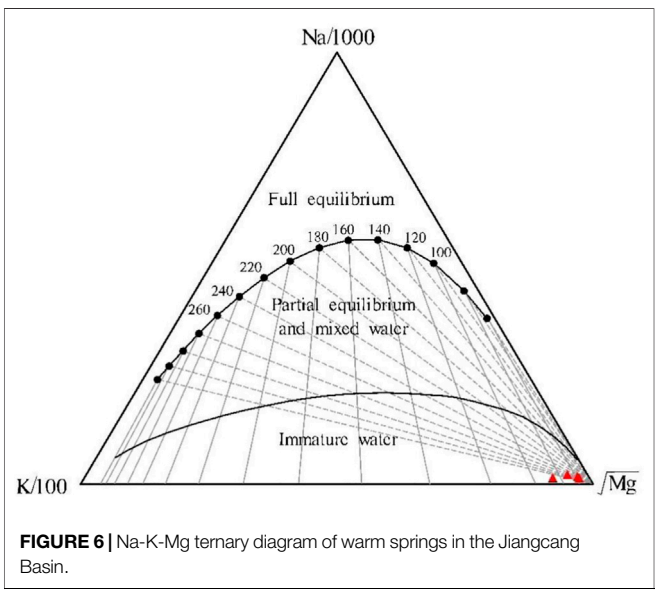

FIGURE 6 | Na-K-Mg ternary diagram of warm springs in the Jiangcang Basin.

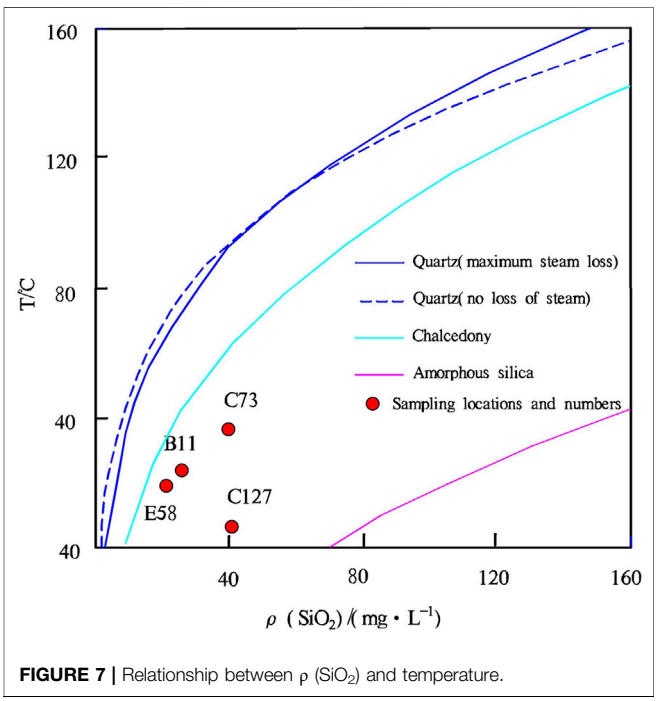

FIGURE 7 | Relationship between ρ (SiO_2) and temperature.

their potential for exploitation and utilization. Geothermometers developed based on the chemical equilibrium of minerals in geothermal fluids can be used to accurately estimate the geothermal reservoir temperature. In this study, the geothermal reservoir temperature in the Jiangcang Basin was estimated using cationic geothermometers, silica geothermometers, and the multi-mineral equilibrium method. Then, properly calculated results were selected for the geothermal reservoir temperature in the basin, based on the analysis of the water-rock mineral equilibrium.

4.3.1 Cationic Geothermometers

Cationic geothermometers are designed to obtain the geothermal reservoir temperature by establishing the relationship between the temperature and the ratio of cations in geothermal water. Commonly used cationic geothermometers include Na-K, K-Mg, and Na-K-Ca geothermometers (Zhao, 1988; Xu and Guo, 2009). The formulas are shown in **Table 3**.

The test results of water samples collected from the four warm springs, the geothermal reservoir temperature was estimated using different cationic geothermometers (Na-K, K-Mg, and Na-K-Ca geothermometers) according to the temperature of spring vents, and the results are listed in **Table 4**. The data in this table show that the calculated results differ too greatly, and thus it is necessary to analyze the applicability of these cationic geothermometers.

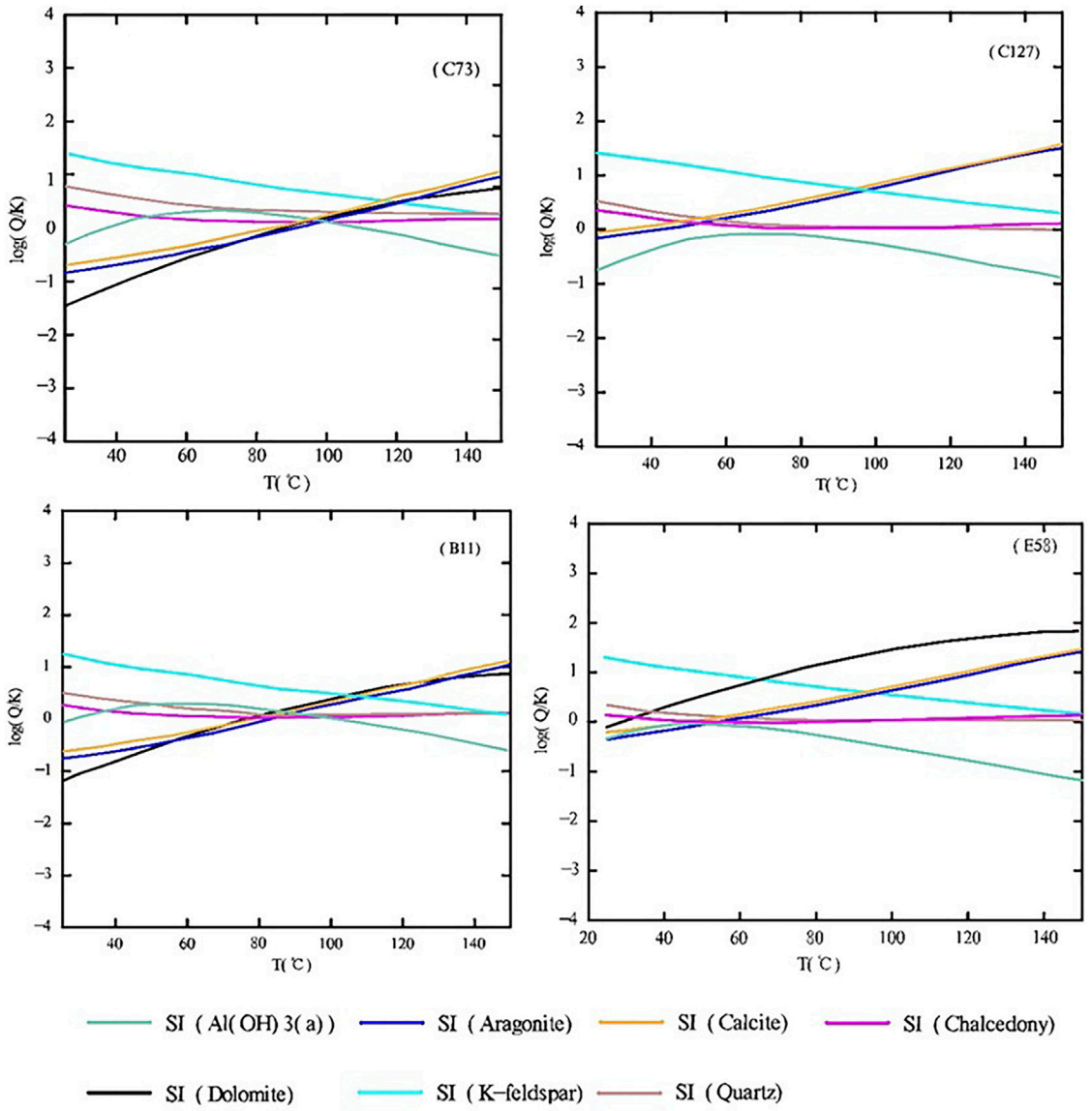

FIGURE 8 | SI-T curves of various minerals in the warm spring water in the Jiangcang Basin.

Different cationic geothermometers should be used in different conditions. The Na-K geothermometer applies to high-temperature geothermal water (temperature >150°C) that is depleted in calcium. Since the warm springs of the Jiangcang Basin feature low temperatures and relatively high Ca^{2+} concentrations (Zhao, 1988), the Na-K geothermometer is not usable. The K-Mg geothermometer applies to low-temperature groundwater. The temperature estimated using the K-Mg geothermometer is generally higher than the temperature of water yielded from a geothermal well and is considered the temperature that can be possibly obtained by drilling toward deep parts (Giggenbach, 1988). A Na-K-Ca geothermometer can be used for medium- and low-temperature Ca-rich water or shallow hot water. This means that the Na-K-Ca geothermometer is the most appropriate for the geothermal reservoirs in the Jiangcang Basin. However, the warm spring water has a generally high Mg^{2+} content, of 38.87–92.5 mg/L. For medium- and low-temperature water rich in Mg^{2+}, the results estimated using the Na-K-Ca geothermometer also significantly deviated from the actual temperatures. Therefore, it is necessary to further correct the estimated results according to the Mg^{2+} content (Rybach and Muffer, 1986).

A geothermometer can be used to estimate the geothermal reservoir temperature on the premise that the minerals in the geothermometer and the minerals in the geothermal reservoir reach equilibrium (Shi et al., 2018). The Na-K-Mg ternary diagram developed based on the Na-K and K-Mg geothermometers can be used to assess the water-rock equilibrium and distinguish different types of water samples. As shown in the Na-K-Mg ternary diagram (**Figure 6**), the water

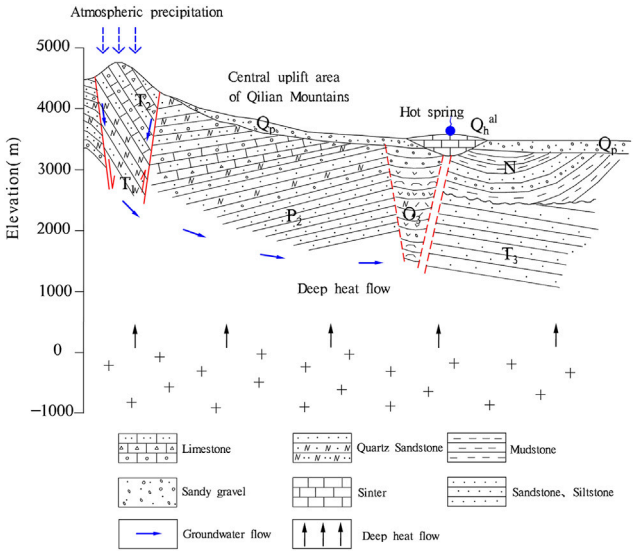

FIGURE 9 | Genetic model of warm spring B11 in the Jiangcang Basin.

samples from the four warm springs in the Jiangcang Basin all fall into the immature water zone. This result indicates that the water-rock interaction in the warm springs has not yet reached an equilibrated state or that the warm spring water is mixed with large amounts of shallow cold water as it rises. In this case, the warm spring water is not sufficiently saturated regarding ion concentrations. Therefore, the geothermal reservoir temperature determined using cationic geothermometers will experience large errors and thus can only be used as a reference.

4.3.2 Silica Geothermometers

Silica geothermometers are used to calculate the temperature of a geothermal reservoir according to the concentrations of silica minerals in hot water since the solubility of silica minerals is a function of temperature. When the temperature is below 300°C, changes in the pressure and salinity have minor effects on the solubility of quartz and amorphous silicon. Moreover, other ions and complexes generally do not affect dissolved silica in water at a temperature of less than 300°C. Therefore, silica geothermometers are one of the most commonly used and effective geothermometers (Zheng and Guo, 1996).

The solubility curves of silica can be used to determine the minerals that control the mass concentration of silica in a solution. There are many types of silica minerals in nature, among which quartz, chalcedony, and amorphous silicon are of primary importance in geothermal study. Based on the relationship between the silica concentration and temperature, as well as the solubility curves of silica (**Figure 7**), the water samples from the warm springs in the study area all fall below the dissolution curves of quartz and chalcedony in the theoretically equilibrated state. This phenomenon indicates that the quartz and chalcedony were oversaturated, but amorphous silicon was not equilibrated in the water samples. Therefore, the silica concentration in the warm springs is possibly controlled by quartz and chalcedony, which can be used to estimate the temperature of deep geothermal reservoirs, as ideal geochemical geothermometers.

Quartz geothermometers can be divided into two types, namely, quartz-no steam loss and quartz-maximum steam loss. Because the study area is at high elevation, 80°C can be considered the boiling point in the area. Given that the four warm springs have a maximum temperature of 36.6°C, the geothermometer of quartz-no steam loss was employed to calculate the temperature of the warm springs in this study, and the equations are as follows:

For geothermometer of quartz-no steam loss: $T=1{,}309/(5.19-\log SiO_2)-273.15$.

For chalcedony geothermometer: $T=1{,}032/(4.69-\log SiO_2)-273.15$.

The calculated results are shown in **Figure 4**.

4.3.3 Multi-Mineral Equilibrium Method

The multi-mineral equilibrium method can be used to determine the chemical equilibrium state of minerals in geothermal fluids. It is designed as follows. Firstly, the dissolution states of multiple minerals in geothermal fluids are expressed as a function of temperature. Then, if several minerals reach equilibrium (saturation index=0) at a certain temperature, the minerals whose equilibrium curves (i.e., the curves formed by connecting the solubility values at different temperatures) converge can be used as geothermometers (Reed and Spycher, 1984; Wu and Sun, 2000), and the temperature obtained is the geothermal reservoir temperature (Chai, et al., 2010). The saturation index (SI) can be used to determine the degree of saturation of minerals. Specifically, values of SI=0, >0, and <0 of minerals indicate that the minerals are saturated, oversaturated, and undersaturated in a solution (Guo and Song, 2005).

The PREEQC software can be used to calculate the SIs of various minerals. Because the rocks in the Jiangcang Basin are dominated by sandstone and are interbedded with shales and limestones, minerals including quartz, chalcedony, K-feldspar, calcite, aragonite, gibbsite, and dolomite were selected to calculate the geothermal reservoir temperature in this study. Then, the SI vs. temperature curves of minerals and geothermal fluids were plotted (**Figure 8**). In this manner, the geothermal reservoir temperature of the study area was obtained (**Table 4**).

As shown in **Figure 8**, K-feldspar and gibbsite curves poorly converge, while the curves of the remaining six minerals converge at a narrow temperature interval and roughly intersect at one point. Moreover, the trend curves of quartz and chalcedony more approximate the curve of SI=0, and the intersection points between the curves of the quartz, chalcedony, and aragonite roughly lie on the curve of SI=0. Therefore, the intersection point of the three types of minerals was used to estimate the geothermal reservoir temperature, and the estimated results are shown in **Table 4**.

The geothermal reservoir temperature, estimated using the multi-mineral equilibrium method was close to that determined using the quartz and chalcedony geothermometers. Because the results obtained using various methods all contain errors, the averages of these results were taken as the temperatures of deep

geothermal reservoirs of the warm springs in the Jiangcang Basin, as shown in **Table. 4**.

4.4 Circulation Depth of Geothermal Water

To obtain a detailed understanding of the genesis of the warm springs in the Jiangcang Basin, the circulation depth of geothermal water was estimated. Geothermal water is usually heated by deep heat sources during deep circulation. The circulation depth of a warm spring can be roughly estimated using the following equation:

$$H = \frac{t - t_0}{k} + H_0 \quad (5)$$

where T is the geothermal reservoir temperature, t_0 is the local average multi-year temperature, k is the geothermal gradient, and H_0 is the thickness of the constant temperature zone. Relevant data reveal that the average annual temperature in the Jiangcang Basin is −5.6°C. As mentioned in the regional hydrogeologic report of the Zhimahe Map Sheet, the logging and temperature data of borehole 8601 lying approximately 2 km to the west of warm spring E58 (No. 958) (i.e., to the west of the Kekesaiqu area) show a temperature gradient of 4.2°C/100m and a thickness of the constant temperature zone of approximately 50 m (Xie et al., 1987). The circulation depths of the geothermal water of warm springs C73, C127, E58, and B11 were calculated to be approximately 2,610 m, 2,276 m, 1848 m, and 2,205 m, respectively. Therefore, all the warm springs in the Jiangcang Basin feature deep circulation, and the warm spring water is mixed with shallow cold water as it rises to the ground surface. In addition, the permafrost in the Jiangcang area has a thickness of up to 86.65 m, causing the geothermal water to cool through conduction as it rises. As a result, the water at the spring vents has a low temperature.

4.5 Genesis Models of Warm Springs

The Jiangcang Basin is a Cenozoic faulted basin, where many warm springs are exposed. The genetic model of the warm springs is exemplified by warm spring B11 (**Figure 9**). B11 is recharged by the atmospheric precipitation and the meltwater from snow and ice in the high mountainous areas on the southwest side of the Jiangcang Basin. The atmospheric precipitation and meltwater from snow and ice infiltrate and migrate downward along regional deep fault F42, which penetrates deep heat sources. The groundwater enters the deep thermal reservoirs through infiltration and recharge by lateral runoff. Then, it is heated by terrestrial heat flow after a long-term and slow deep circulation, forming deep geothermal resources. Faults serve as pathways with effective hydraulic conductivity. There are more than 30 faults and folds of various sizes in the study area. Influenced by faults and the water blocking of the Nanyinger Formation (T3n) and Paleogene (N) mudstones, geothermal water rises along faults and is mixed with shallow groundwater as it rises. Finally, the mixed water is exposed as a low-temperature warm spring in the muddy gravels (Q2) of the moraine mound zone in the piedmont.

The geothermal water of B11 mainly originates from the heat flow conduction of deep granites and natural geothermal gradients. As indicated by the isotopic analysis, the geothermal water of B11 is primarily recharged by atmospheric precipitation and meltwater from snow, with a recharge elevation of 4,401–4,501 m and a circulation depth of up to 1,848–2,610 m. Tectonic fractures of Triassic sandstones serve as the water-bearing media of the geothermal water of B11. The water in these tectonic fractures is characterized by long circulation pathways, strong water-rock interaction, and high TDS. The deep geothermal water is mixed with the shallow cold water and is cooled by the upper permafrost through conduction. Finally, the mixed water is exposed as the Zemoyesang low-temperature warm spring.

5 CONCLUSION

(1) The warm springs in the Jiangcang Basin have hydrochemical types of HCO_3-Ca·Mg, HCO_3-Ca·Na·Mg, and HCO_3·SO_4-Na·Ca. Hydrochemical analyses show a high correlation between $Mg^{2+}$and TDS, with a correlation coefficient of up to 0.96. By contrast, there is a low correlation between Na^{2+} and TDS, with a correlation coefficient of 0.65. These results reflect the ion composition characteristics of medium- and low-temperature thermal springs. Moreover, there is no significant positive correlation between Cl^- and other ions in the warm springs, indicating that the trace elements in the warm springs mainly originate from the dissolution of relevant minerals.

(2) The points of δ^2H and $\delta^{18}O$ values of water samples from the Jiangcang Basin all fall below the LMWL, indicating different degrees of $\delta^{18}O$-shift. By comparison with the average $\delta^{18}O$ value of the local atmospheric precipitation, the $\delta^{18}O$-shift of the cold water is mainly affected by evaporation, while that of the warm springs is primarily caused by deep water-rock interactions.

(3) The temperature of the deep geothermal reservoirs in the Jiangcang Basin is 51–83°C, with an average of 67°C. The results of the calculations of the hydrogen and oxygen isotopes show that the recharge elevation of the warm springs is 4,401–4,501 m (average: 4450 m), which is similar to the elevation of the Tuolai Nanshan Mountain and the Datong Mountain on the north and south sides of the Jiangcang Basin, respectively. Therefore, the warm spring water in the study area is mainly recharged by atmospheric precipitation and meltwater from snow of the piedmont. In addition, the circulation depth of the geothermal water is 1,848–2,610 m.

(4) The atmospheric precipitation and meltwater from ice and snow infiltrate downward through the deep fault fracture zones in the high mountainous areas and then form runoff in the basin along the tectonic channels. Then, they are heated through deep circulation and then rise along faults under the influence of fault structures and the water blocking of mudstones. As they rise, they are mixed with the shallow groundwater and cool by the upper permafrost through

conduction. Finally, the mixed water is exposed as low-temperature tectonic warm springs.

DATA AVAILABILITY STATEMENT

The original contributions presented in the study are included in the article/supplementary material, and further inquiries can be directed to the corresponding author.

AUTHOR CONTRIBUTIONS

LL was responsible for numerical simulation and drafting the paper. WW put forward the research idea. YZ and MG helped with the field survey and sampling. SQ gave guidance regarding the genetic model of the warm springs. JH assisted in data analysis.

FUNDING

This research was supported by the Natural Science Foundation of China (41502336), the China Geological Survey Grant (DD20221676), and the S&T Program of Hebei Province, China (No. 20374201D).

ACKNOWLEDGMENTS

We would like to extend our gratitude to Researcher Xiangquan Li and Senior Engineer Zhenxing Wang from the Institute of Hydrogeology and Environmental Geology, Chinese Academy of Geological Sciences, for their assistance in data and materials. Our thanks also go to Researcher Wenjing Lin, Associate Researcher Zhaoxian Zheng, and Associate Researcher Xiaojiao Guo for their great assistance in mapping and article polishing.

REFERENCES

Chai, R., Wang, H., and Liu, Y. (2010). Application of Multimineral Balance Method to Estimation of Geothermal Temperature. *Coal Sci. Technol.* 38 (4), 100–103. doi:10.13199/j.cst.2010.04.107.chair.001 (in Chinese with English abstract).

Chen, L. (2019). Isotopic Characteristics Analysis of Hydrogenoxygen Environment in Geothermal Water in Fujian Province. *Geology of Fujian* 1, 61–68. (in Chinese with English abstract).

Dai, M. (2020). "The Hydrogeochemical Characteristics and the Evolution of Geothermal Water in Guide Area, Qinghai," (Beijing: China university of geosciences). Master's thesis.

Du, G. L., Cao, W. H., and Zhai, B. (2012). Genesis of Baoquantang Hot Spring and its Influence on Fault and Seismicity in Weihai City. *Mar. geology&Quaternary Geol.* 32 (5), 67–72. doi:10.3724/SP.J.1140.2012.05067

Giggenbach, W. F. (1988). Geothemal Solute Equilibria. Derivation of Na-K-Ca Geoindicators. *Geochim. Cosmochim. Acta* 52, 2749–2765. doi:10.1016/0016-7037(88)90143-3

Guo, Z. J., and Song, H. Z. (2005). Chemical Components in Groundwater and its SI Values. *Resources Environment & Engineering* 19 (3), 200–202.

Guo, Z. J., Wang, J. G., Chen, Z., and Shi, J. H. (2015). Discussion on the Formation Mechanism of Wenshui Longtan Hot Spring in Xishan, Heqing, Yunnan Province. *Geotech. Investig.* 5, 43–48.

Jiang, Z. J., Xu, T. F., Dirk, M., Tian, H., and Owen, D. D. R. (2019). Numerical Modelling of Stable Isotope (2H and 18O) Transport in a Hydro-Geothermal System: Model Development and Implementation to the Guide Basin, China. *J. Hydrology* 569 (2), 93–105. doi:10.1016/j.jhydrol.2018.11.065

Lang, X. J., Lin, W. J., Liu, Z. M., Xing, L. X., and Wang, G. L. (2016). Hydrochemical Characteristics Water in Guide Basin. *Earth Sci.* 41 (10), 1723–1734.

Li, H. D., Zhang, S. Q., Bai, J. Q., Zhou, J. Y., Shi, W. D., and Zhao, Y. (2007). Hydrochemistry and Origin of the Yaoshuitan Geothermal Field, Xining, Qinghai. *Acta Geol. Sin.* 81 (9), 1299–1304.

Li, X. Q., Hou, X. W., Wang, Z. X., Liu, L. X., Gao, M., Ma, J. F., et al. (2016a). *Institute of Hydrogeology and Environmental Geology*. China: Chinese Academy of Geological Sciences. 1:50,000 hydrogeological map manual of the Jiariguorixue.

Li, X. Q., Wang, Z. X., Hou, X. W., Chen, J., Liu, L. X., Gao, M., et al. (2016b). *Institute of Hydrogeology and Environmental Geology*. China: Chinese Academy of Geological Sciences. Hydrogeology and environmental geology survey report of important energy base in Qinghai province.

Li, L. L. (1952). "Research on the Preservation Law and Genetic Model of Geothermal Resources in Guide Basin , Qinghai Province," (China: East china university of technology). Master's thesis.

Li, Y. G. (2016). "Hydrogeochemical Characteristics and its Origin Analysis of Geothermal Water in the Qia Bu-Qia Area, Gonghe Basin, Qinghai Province," (China: East china university of technology). Master's thesis.

Ma, Y. H., Tang, B. C., Su, S. Y., Zhang, S. S., and Li, C. Y. (2020). Geochemical Characteristics of Geothermal Fluids and Water-Rock Interaction in Geothermal Reservoirs in and Around the Gonghe Basin, Qinghai Province. *Earth Sci. Front.* 27 (1), 123–133. doi:10.13745/j.esf.2020.1.14

Ni, G. Q., Zhang, H., Wei, Y. T., and Hu, Y. Z. (2016). Hydrogeochemical and Isotope Characteristics of Geothermal Fluid in Sichuan. *Adv. New Renew. Energy* 4 (3), 184–194. doi:10.3969/j.issn.2095-560X.2016.03.004

Reed, M., and Spycher, N. (1984). Calculation of pH and Mineral Equilibria in Hydrothermal Waters with Application to Geothermometry and Studies of Boiling and Dilution. *Geochimica Cosmochimica Acta* 48 (7), 1479–1492. doi:10.1016/0016-7037(84)90404-6

Rybach, L., and Muffler, L. J. P. (1986). *Geothermal Systems - Principles and Analysis of Typical Geothermal Systems*. China: Department of Geology, Peking University. Translated by the Geothermal Research Unit.

Shi, J., Nai, W. H., Li, M., Wang, S., Ma, X. J., and Zhang, J. (2018). Hydrogeochemical Characteristics of High Temperature Geothermalfield of the Quman Geothermal Field in Xinjiang. *Hydrogeology & Engineering Geol.* 45 (3), 165–172. doi:10.16030/j.cnki.Issn.1000-3665.2018.03.23

Sun, Z. X., Li, X. L., and Shi, W. J. (1992). Isotopic Hydrogeochemistry of Mid-low Temperature Geothermal Water in Jiangxi Province. *J. East China Geol. Inst.* 15 (3), 243–248.

Sun, C. J., Zhang, Z. Y., Chen, W., Li, W., Chen, R. X., School of Geographical Science, et al. (2019). Spatial Distribution of Precipitation Stable Isotopes in the Alpine Zones in Central Asia. *Arid Zone Res.* 36 (01), 19–28. doi:10.13866/j.azr.2019.01.03

Sun, H. L., Wang, G. L., and Lin, W. J. (2022). Distribution Characteristics and Enrichment Mechanism of TDS Geothermal Water in Xining Basin. *Bull. Geol. Sci. Technol.* 41 (1), 278–287. doi:10.19509/j.cnki.dzkq.2021.0079

Tang, X. C., Wang, G. L., Ma, Y., Zhang, D. L., Liu, Z., Zhao, X., et al. (2020). Geological Model of Heat Source and Accumulation for Geothermal Anomalies in the Gonghe Basin, Northeastern Tibetan Plateau. *Acta Geol. Sin.* 94 (7), 2052–2065. doi:10.1111/1755-6724.14541

Wang, G. L., Zhang, W., Liang, J. Y., and Lin, W. J. (2017a). Evaluation of Geothermal Resources Potential in China. *Acta Geosci. Sin.* 38 (4), 449–459. doi:10.3975/cagsb.2017.04.02

Wang, G. l., Zhang, W., Lin, W. J., Liu, F., and Zhu, X. (2017b). Research on Formation Mode and Development Potential of Geothermal Resources in Beijing-Tianjin-Hebei Region. *Geol. China* 44 (6), 1074–1085. doi:10.12029/gc20170603

Wang, R. J. (2009). Geochemical Characteristics and Resource Evaluation of Underground Hot Water in the Chabcha Geothermal Zone of the

Republican Basin, Qinghai Province. (China: Chang'an University). Master's thesis.
Wu, H. M., and Sun, Z. X. (2000). Calculation of the Fluid-Rock Equilibrium State in the Geothermal System. *J. east china Geol. Inst.* 23 (1), 39–42.
Xie, C. J., Liu, Z. F., Xu, X. C., and Zhang, S. Q. (1987). *Second Hydrogeological Team of Qinghai Province*. 1:200,000 regional hydrogeological survey report of the zhihema.
Xu, S. G., and Guo, Y. S. (2009). *Fundamentals of Geothermics*. Beijing: Science Publishers.
Yang, S. K., Luo, Y. F., Zhao, Z., Zhang, S. S., Zhang, Z. X., A., H. J., et al. (2015). Report on the Evaluation and Zoning of the Current Situation of Geothermal Resources in Qinghai Province. Xining: Qinghai Bureau of Environmental Geology Exploration.
Yang, Y. F. (2019). "Precipitation and Runoff Process in Shaliu River Basin of Qinghai Lake Based on Hydrogen-Oxygen Stable Isotope Technique," (China: Qinghai Normal University). Master's thesis.
Yuan, X. f., Wang, J., Huo, G., Song, M. z., and Wang, J. l. (2020). Hydrochemistry and Genesis of the Hongshuilantang Hot Spring in the Jiaodong Peninsula. *Geol. Explor.* 56 (2), 427–437. doi:10.12134/j.dzykt.2020.02.017
Yuan, J. (2010). "Transport of Boron in the Aquatic Environment of the Yangbajing Geothermal Field, Tibet," (China: China University of Geosciences). Master's thesis.
Zhang, S. Q., Li, H. D., Xu, G. C., Shi, W. D., Zhou, J. Y., and Shang, X. G. (2007). Geochemical Characteristics of Groundwater in the Du Jia Zhuang Geothermal Field in the South of xining、Qinghai. *Front Earth Science*. 21 (1), 163–169.
Zhang, C. C., Li, X. Q., Ma, J. F., Fu, C. C., and Bai, Z. X. (2021). Formation Pattern of Geothermal Water in Chaya of Tibet Based on Hydrochemistry and Stable Isotopes. *Geoscience* 35 (1), 1–22. doi:10.19657/j.geoscience.1000-8527.2021.013
Zhang, X. G. (1988). Application of Isotopic Geochemistry in Geothermal Exploration. *Hydrogeology Eng. Geol.* 1, 28–31.
Zhang, Z. (1999). Rich Geothermal Resources in Qinghai. *Earth* 6, 11.
Zhao, Q. S. (1988). The Application of Geothermometers in the Exploration of Hydrothermal Resources in Western Sichuan. *J. chengdu Univ. Sci. Technol.* 37 (1), 44–50.
Zheng, X. L., and Guo, J. Q. (1996). Silica Geothermal Temperature Scale and its Related Treatment Methods. *Groundwater* 18 (2), 85–88.

Conflict of Interest: The authors declare that the research was conducted in the absence of any commercial or financial relationships that could be construed as a potential conflict of interest.

The handling editor WL declared a shared affiliation with the authors LL, MG, and WW at the time of review.